



Tavorite Lithium Iron Fluorophosphate Cathode Materials: Phase Transition and Electrochemistry of LiFePO_4F – $\text{Li}_2\text{FePO}_4\text{F}$

T. N. Ramesh, Kyu Tae Lee, B. L. Ellis, and L. F. Nazar^{*,z}

Department of Chemistry, University of Waterloo, Waterloo, Ontario N2L 3G1, Canada

We have synthesized LiFePO_4F by a simple solid-state route as a pure single phase, which we show is isostructural with that of the minerals tavorite and amblygonite, and we report the first isolation of its fully lithium-inserted crystalline analog, $\text{Li}_2\text{FePO}_4\text{F}$.

We show that the latter adopts a triclinic $P\bar{1}$ tavorite-type framework that is very closely related to the parent phase. The redox activity between these two compositions is very facile and occurs with an 8% change in volume to result in a reversible and stable capacity of about 145 mAh/g. The electrochemical cycling at both room temperature and 55°C is very stable.

© 2010 The Electrochemical Society. [DOI: 10.1149/1.3298353] All rights reserved.

Manuscript submitted December 1, 2009; revised manuscript received December 29, 2009. Published February 3, 2010. This was Paper 397 presented at the Vienna, Austria, Meeting of the Society, October 4–9, 2009.

The family of lithium transition-metal phosphates and fluorophosphates is acquiring increasing importance as positive electrode materials for safe and low cost lithium-ion cells. Among this family, olivines have commanded much attention in the past decade, accounting for well over 1000 published papers, but far fewer materials have been developed that exhibit similarly attractive features. In the search for structural frameworks that overcome the one-dimensional (1D) ion conductivity challenge of olivine, we have turned to the tavorite family. These materials $\text{LiMPO}_4(\text{OH})_x\text{F}_{1-x}$ ($M = \text{Al, Ga, V, Fe, Mn, and Ti}$) crystallize in the triclinic space group $P\bar{1}$. Those composed of M^{3+} ions, which are abundant in the earth's crust such as Fe^{3+} and Al^{3+} , are found in nature as the minerals montebrasite (LiAlPO_4OH),¹ amblygonite (LiAlPO_4F),² and tavorite (LiFePO_4OH).³ They form a large, fascinating, and isostructural family of alkali metal fluoro(hydroxyl) phosphates with variable F^-/OH^- content, which possess multidimensional pathways for Li^+ migration. The substitution of fluorine for hydroxyl moieties is best known in the calcium hydroxyapatites, minerals such as $\text{Ca}_5\text{Al}(\text{PO}_4)_3(\text{OH},\text{F})$ that form the basis of bones and teeth.⁴ In these minerals, the F^- substitution (“fluoridation”) renders structural stability, whereas in electrochemical materials, the complete F^- substitution is critical for redox stability to overcome the irreversible electrochemical activity of the hydroxyl group. The fluorosulfates, LiMgSO_4F and $\text{FeSO}_4(\text{OH})$, also fall into exactly the same tavorite/amblygonite structure type, with the former possessing good ion conductivity⁵ and the latter reported to be a promising host for lithium insertion.⁶

In contrast to olivine, tavorite possesses 1D chains of FeO_6 that result in 1D electron transport, with intersecting channels housing Li^+ that afford open pathways for three-dimensional (3D) ion transport. The material LiVPO_4F , demonstrated to be a viable cathode in Li-ion batteries,⁷ is also suggested to be a member of the same tavorite–amblygonite family, although detailed structural data were not reported. LiFePO_4F represents a new fluorophosphate member of this family that was also mentioned earlier, but neither preparative, structural, nor electrochemical data were reported.⁸ As part of our continuing quest for new fluorophosphates,⁹ here we demonstrate that LiFePO_4F can be easily synthesized by solid-state routes, although not by the method described previously. We have isolated it as a pure single phase, which we show is isostructural with that of tavorite, and have obtained its reduced form, $\text{Li}_2\text{FePO}_4\text{F}$, as a single phase, as described previously.¹⁰ We show that the latter also adopts a very closely related triclinic $P\bar{1}$ tavorite-type framework that ex-

hibits about an 8% increase in the unit cell volume. The redox activity between these two phases is very facile and results in a reversible capacity of about 145 mAh/g. The electrochemical cycling at both room temperature and 55°C is very stable in over at least 40 cycles.

Experimental

LiFePO_4F was prepared from the reaction of FePO_4 with LiF (1:1 mol ratio). First, FePO_4 was synthesized by the reaction of stoichiometric quantities of Fe_2O_3 and diammonium hydrogen phosphate at 870°C for 6–10 h. FePO_4 was then ballmilled with LiF and heated at 575°C for 75 min in an argon flow. The material can also be prepared by the reaction of stoichiometric quantities of FePO_4 , NH_4F , and Li_2CO_3 at 575°C for 90 min in an argon flow.

$\text{Li}_2\text{FePO}_4\text{F}$ was prepared by adding LiFePO_4F to a solution of lithium aluminum hydride (1:1.5 mol ratio) in tetrahydrofuran. The mixture was stirred for 44 h at 25°C in an inert atmosphere, and the product was filtered and dried. The chemical oxidation of $\text{Li}_2\text{FePO}_4\text{F}$ was accomplished by oxidation with NOBF_4 in a five-fold molar excess in acetonitrile for 5 h in an inert atmosphere. The product was filtered, washed with acetonitrile, and dried under ambient conditions.

X-ray diffraction (XRD) measurements were performed on a Bruker D8 Advance powder diffractometer using $\text{Cu K}\alpha$ radiation ($\lambda = 1.5405 \text{ \AA}$) from $2\theta = 10\text{--}80^\circ$ at a count rate of 10 s per step of 0.02° . The XRD pattern of $\text{Li}_2\text{FePO}_4\text{F}$ was collected using a hermetically sealed holder owing to its air sensitivity. Refinement was carried out using GSAS software.¹¹ The cell parameters were first determined by the LeBail pattern matching for LiFePO_4F or by indexing for $\text{Li}_2\text{FePO}_4\text{F}$. A subsequent Rietveld refinement analysis was carried out initially using fractional coordinates from either LiFePO_4OH or LiGaPO_4OH .^{3,12} Scale factor, zero point, lattice parameters, atomic positions, and thermal factors were iteratively refined. The elemental analysis of the samples was carried out using inductively coupled plasma and energy dispersive X-ray analysis (EDX) in the scanning electron microscope (SEM).

For electrochemistry studies, LiFePO_4F was ballmilled with carbon (Super S, MMM) in a planetary high speed mill for 2 h. The paste comprised of LiFePO_4F , Super S, and poly(tetrafluoroethylene) in a weight ratio of 70:20:10 was pressed onto carbon-coated Al foil and was dried at 80°C overnight in a vacuum oven. Electrochemical cells were constructed using a coin-cell design, utilizing 1 M LiPF_6 /ethylene carbonate/dimethyl carbonate (1:1) (Merck) as the electrolyte and about 6 mg of active material. Cells were assembled in a glove box under Ar with O_2 and H_2O lower than 5 ppm. Cells were cycled between 1.5 and 4.0 V in the galvanostatic mode at room temperature and at 55°C with a current density equivalent to a C/10 rate.

* Electrochemical Society Active Member.

^z E-mail: lfnazar@uwaterloo.ca

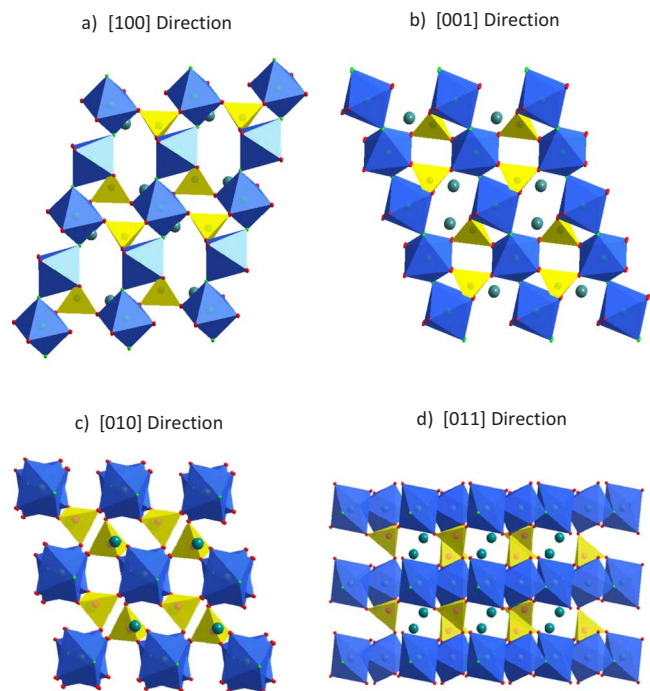


Figure 1. (Color online) Structure of the tavorite phase of LiFePO_4F based on the structural refinement in Fig. 2a. (a) View down $[100]$, (b) view down $[001]$, (c) view down $[010]$, and (d) view down $[011]$. The iron and phosphorus coordination environments are represented as octahedra and tetrahedra, respectively and lithium ions as large spheres.

Results and Discussion

Our methodology to form LiFePO_4F differs from the previously reported synthesis via the reaction of the same reagents in air at 700°C ,⁸ which in our hands produces predominantly $\text{Li}_3\text{Fe}_2(\text{PO}_4)_3$ and $\alpha\text{-Fe}_2\text{O}_3$ (hematite). We find that the solid-state reaction of FePO_4 and LiF in N_2 at 575°C yields LiFePO_4F , whose structure derived from the analysis of the powder pattern is depicted in Fig. 1. The XRD pattern and Rietveld analysis of LiFePO_4F , using the tavorite LiFePO_4OH model in $P\bar{1}$ as a starting point (Fig. 2a), indicate that, essentially, a single-phase material is formed.

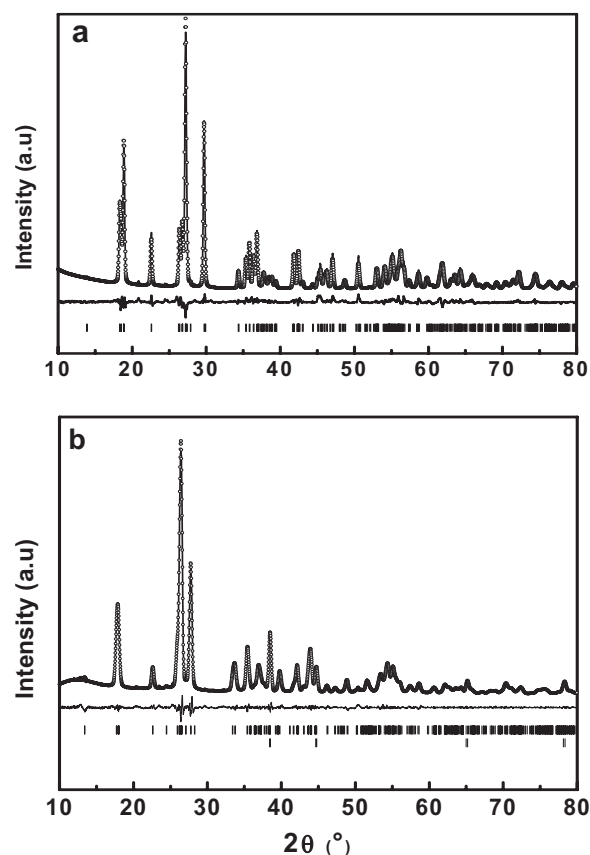


Figure 2. Comparison of the experimental (α) and calculated ($-$) XRD patterns for (a) LiFePO_4F , Rietveld refinement in $P\bar{1}$; (b) the reduced phase, $\text{Li}_3\text{Fe}_2\text{PO}_4\text{F}$, LeBail refinement in $P\bar{1}$. The positions of the (hkl) reflections and the difference curve are also shown. The framework atomic coordinates from the tavorite model were used as a starting point for the Rietveld refinement. The second phase in the pattern of $\text{Li}_3\text{Fe}_2\text{PO}_4\text{F}$ is from elemental aluminum arising from the reaction of LiFePO_4F with LiAlH_4 .

$\text{Li}_3\text{Fe}_2(\text{PO}_4)_3$ is typically present as approximately 1–2% impurity that arises from a slight decomposition of LiFePO_4F , which is more

Table I. Lattice parameters for LiFePO_4F and $\text{Li}_2\text{FePO}_4\text{F}$ from XRD refinement.

| Sample | a (\AA) | b (\AA) | c (\AA) | α ($^\circ$) | β ($^\circ$) | γ ($^\circ$) | V (\AA^3) |
|------------------------------------|-------------------------|-------------------------|-------------------------|--------------------------|-------------------------|--------------------------|---------------------------|
| $\text{Li}_2\text{FePO}_4\text{F}$ | 5.3746(3) | 7.4437(4) | 5.3256(4) | 109.038(2) | 94.423(6) | 108.259(9) | 189.03(4) |
| LiFePO_4F | 5.3002(2) | 7.2601(2) | 5.1516(2) | 107.880(3) | 98.559(3) | 107.343(3) | 173.67(6) |

Table II. Structural data for LiFePO_4F based on Rietveld refinement shown in Fig. 2a.

| Atom | Wyckoff position | x | y | z | Occupancy | U_{iso} (\AA^3) |
|---------------|------------------|------------|-----------|-----------|-----------|--|
| Li_1 | 2i | 0.6309(6) | 0.2960(5) | 0.2569(7) | 0.77 | 0.02631(7) |
| Li_2 | 2i | 0.6037(2) | 0.1834(1) | 0.2319(2) | 0.23 | 0.02631(7) |
| Fe_1 | 1c | 0 | 0.5 | 0 | 1.0 | 0.00967(1) |
| Fe_2 | 1a | 0 | 0 | 0 | 1.0 | 0.00936(1) |
| P | 2i | 0.6441(8) | 0.7504(7) | 0.3174(8) | 1.0 | 0.01633(7) |
| O_1 | 2i | 0.6622(1) | 0.8612(1) | 0.1125(2) | 1.0 | 0.01396(7) |
| O_2 | 2i | 0.3533(2) | 0.6393(1) | 0.3232(2) | 1.0 | 0.01403(7) |
| F | 2_i | 0.9162(2) | 0.2592(1) | 0.1234(1) | 1.0 | 0.01403(7) |
| O_3 | 2i | 0.79347(1) | 0.5962(1) | 0.2844(1) | 1.0 | 0.01401(7) |
| O_4 | 2i | 0.23774(1) | 0.0771(1) | 0.3789(1) | 1.0 | 0.01420(7) |

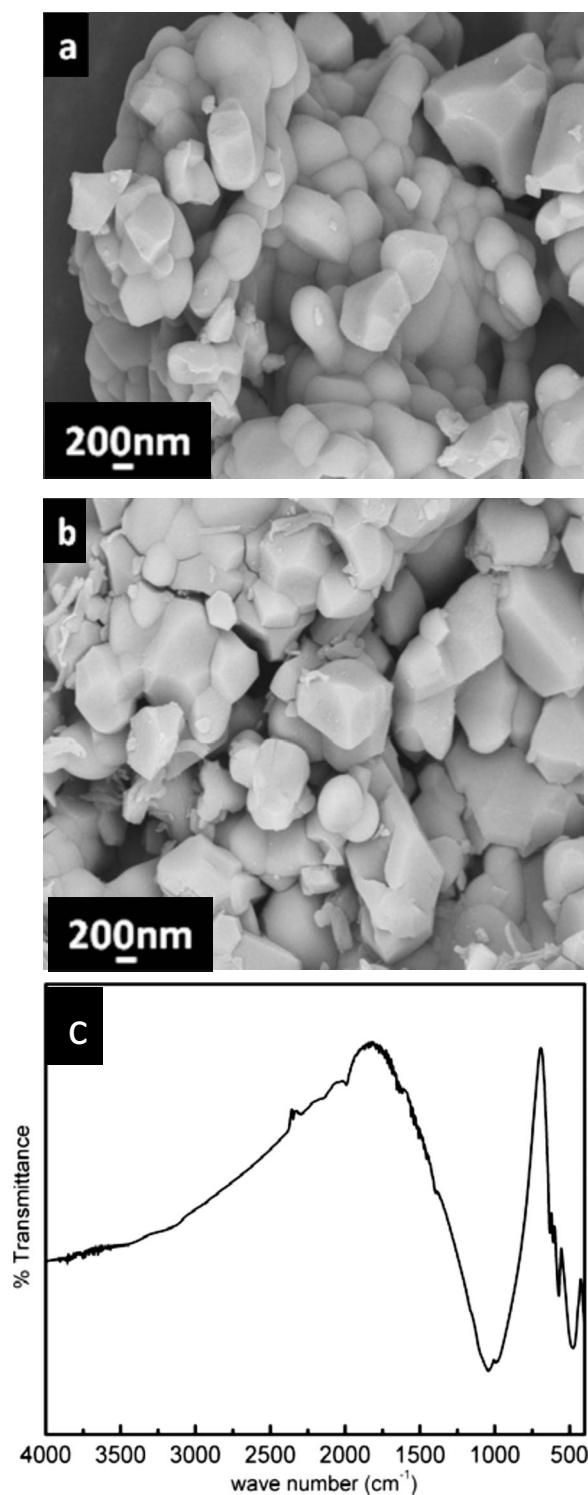


Figure 3. Field-emission-scanning electron microscope micrographs of (a) LiFePO_4F , (b) $\text{Li}_2\text{FePO}_4\text{F}$, and (c) IR spectrum of LiFePO_4F .

notable using synthesis temperatures above 600°C . During the submission of this work, we also became aware of the synthesis of LiFePO_4F by the reaction of FeF_3 and Li_3PO_4 either by a solid-state reaction in sealed Pt tubes at 700°C or in ionic liquid media at 260°C and of its structural resolution.¹³ In both cases, the formation of LiF as a by-product helps to force the reaction to completion, but it is not completely extractable, as seen in the diffraction patterns.

The refinement converged with good statistics ($R_{\text{wp}} = 9.9$, R_{p}

Table III. Bond lengths for LiFePO_4F based on Rietveld refinement shown in Fig. 2.

| LiFePO_4F (split Li sites) | | Bond length (\AA) |
|--|------------------------|------------------------------|
| Fe_1 | $\text{F}(\times 2)$ | 1.9902 |
| | $\text{O}_3(\times 2)$ | 2.0346 |
| | $\text{O}_2(\times 2)$ | 2.0507 |
| Fe_2 | $\text{O}_4(\times 2)$ | 1.9721 |
| | $\text{F}(\times 2)$ | 1.9985 |
| | $\text{O}_1(\times 2)$ | 2.0361 |
| P | O_1 | 1.5101 |
| | O_2 | 1.5231 |
| | O_3 | 1.5372 |
| | O_4 | 1.5646 |
| Li_1 | O_1 | 2.0172 |
| | O_2 | 2.0542 |
| | O_3 | 2.0414 |
| | O_4 | 2.5028 |
| Li_2 | F | 1.8081 |
| | O_1 | 1.9658 |
| | O_1 | 2.3530 |
| | O_2 | 2.1963 |
| F | O_3 | 2.7723 |
| | O_4 | 2.1993 |
| | | 1.8105 |
| | | |

= 7.2) with or without the inclusion of the minor impurity phase. The lattice parameters summarized in Table I, fractional coordinates (Table II) and selected bond lengths (Table III) agree with other members of the tavorite-amblygonite family [$a = 5.3002(2)$ \AA , $b = 7.2601(2)$ \AA , $c = 5.1516(2)$ \AA , $\alpha = 107.880(3)^\circ$, $\beta = 98.559(3)^\circ$, $\gamma = 107.343(3)^\circ$, and $V = 173.67(6)$ \AA^3] and are similar to those independently reported.¹³ The SEM micrograph indicates that the particle size is about 1 μm (Fig. 3b). The IR spectroscopy (Fig. 3c) shows the bands expected for phosphate moieties (between 950 and 1100 cm^{-1}) and, importantly, demonstrates the complete absence of hydroxyl groups in the region around 3000–3300 cm^{-1} . Their absence in the lattice is critical to the electrochemical reversibility. The EDX and chemical analysis reveal that the Li/Fe/P/F mole ratio for LiFePO_4F and $\text{Li}_2\text{FePO}_4\text{F}$ are 1:1:1:1, and that for $\text{Li}_2\text{FePO}_4\text{F}$ is 2.2:1:1:1. The additional Li content for $\text{Li}_2\text{FePO}_4\text{F}$ results from some residual Li salt on the surface.

In this tavorite framework, the (FeF_2O_4) octahedra form corner-sharing 1D chains in the [010] direction with alternating tilted octahedra bridged by the F^- ligands. These chains are connected by corner-sharing the phosphate tetrahedra to create a spacious 3D framework; namely, tunnels (>4 \AA in diameter) are present along all of the (100), (010), (001), and (011) directions. The lithium ions reside in the largest tunnels located along the (100) direction, which have a diameter of 5.6 \AA . These tunnels intersect another series, 4.6 \AA in diameter, that run along the [001] direction, as shown in Fig. 1b. The network of tunnels explains the high ionic conductivity displayed by these materials. The lithium site forms a large distorted octahedron. The previous single-crystal structural reports of amblygonites have refined it as a split position between two sites that are occupied either at 50:50 or close to 75:25, which in LiFePO_4OH are 0.76 \AA apart. Alternatively, this would represent a large anisotropic thermal parameter along the direction of the split, indicating that lithium is loosely bound, although the X-ray refinement does not allow this distinction. Isostructural LiGaPO_4OH has also been refined with a single occupancy lithium site on the basis of the powder X-ray data.¹² We carried this out as well and found that the Fe–P–O framework is essentially identical in either case. We report our refinement based on the split Li site based on the fact that the goodness-of-fit is slightly better. Despite the presence of two crystallographically distinct Fe sites in the $P\bar{1}$ lattice, their very similar

environment gives rise to a Mössbauer spectrum with only one resolved single site. The fitted parameters [isomer shift (IS) of 0.42(1) mm/s and quadrupole splitting (QS) of 1.15(1) mm/s] agree with values for Fe^{3+} in an octahedral setting, as expected.

The complete extraction of Li from LiVPO_4F has been reported to form VPO_4F at 4.1 V, a voltage characteristic of the V (III–IV) couple. Significant extraction of Li from LiFePO_4F is not likely though because the Fe (III–IV) potential lies too high for oxidation at accessible potentials. Nonetheless, lithium can be readily inserted in the structure to give a single-phase $\text{Li}_2\text{FePO}_4\text{F}$. This can be accomplished by reduction using either LiAlH_4 or BuLi. The chemical analysis and EDX analysis in SEM confirmed a Li/Fe ratio of 2:1. Mössbauer spectroscopy confirmed the presence of Fe^{2+} in the lattice. On reduction, the pattern is split into two signals with (i) IS = 1.20(1) mm/s; QS = 2.17(3) mm/s and (ii) IS = 1.23(3) mm/s; QS = 2.79(7) mm/s, both typical of Fe^{2+} in an octahedral setting. The two sites in the parent tavorite lattice thus become much more diverse in a coordination environment vis-à-vis the parent phase. The same diffraction pattern is obtained for $\text{Li}_2\text{FePO}_4\text{F}$, irrespective of how it is prepared, although the reflections are slightly sharper in the LiAlH_4 reduction. The SEM image also shows that the particle crystallinity and morphology are retained upon reduction, without any crystallite degradation (Fig. 3d). The XRD data (Fig. 2b) were refined with good reliability factors ($R_{\text{wp}} = 8.0\%$, $R_p = 5.9\%$). They show that the introduction of the second lithium does not result in a large change in the global structural framework features based on the strong similarity in the lattice parameters of the oxidized and reduced phases (Table I). The $P\bar{1}$ space group is maintained in $\text{Li}_2\text{FePO}_4\text{F}$ with a lattice parameter

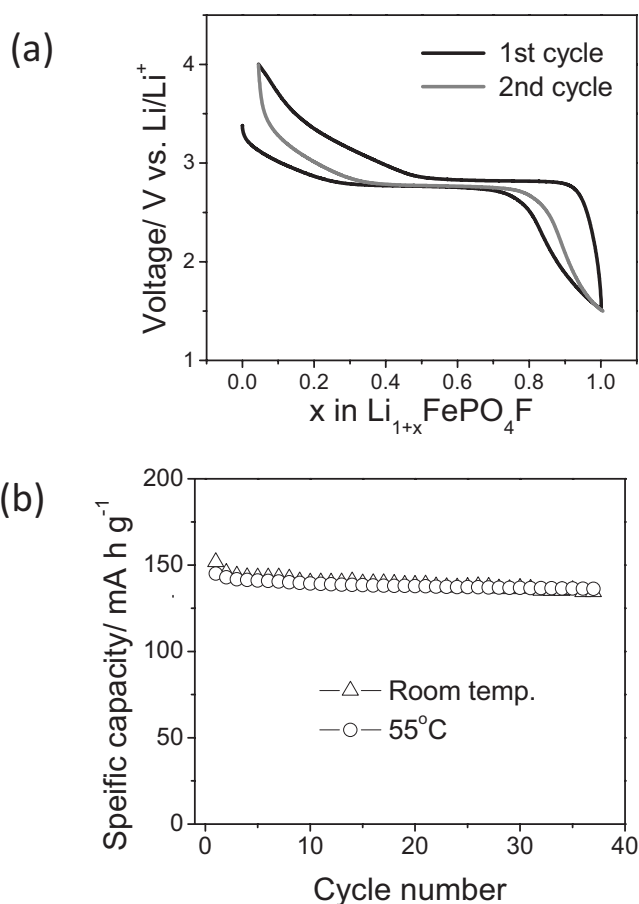


Figure 4. (a) Electrochemical discharge–charge profiles of LiFePO_4F at a cycling rate of C/10 (room temperature) and (b) cycling performance at room temperature and at 55°C .

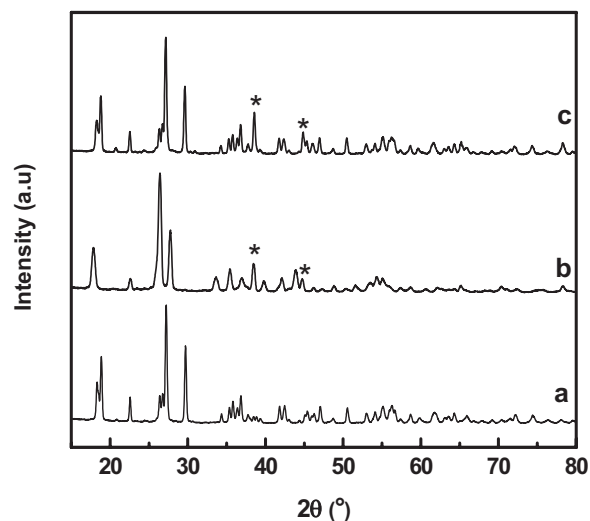


Figure 5. Powder XRD patterns illustrating the reversible chemical changes upon “chemical” cycling: (a) LiFePO_4F , (b) $\text{Li}_2\text{FePO}_4\text{F}$ on reduction with LiAlH_4 , and (c) LiFePO_4F generated upon oxidation of $\text{Li}_2\text{FePO}_4\text{F}$. The reflections marked with an asterisk are from elemental aluminum in the sample arising from the reaction of LiFePO_4F with LiAlH_4 , which persist in the reoxidized phase of LiFePO_4F .

characteristic of an expanded tavorite: $a = 5.3746(3) \text{ \AA}$, $b = 7.4437(4) \text{ \AA}$, $c = 5.3256(4) \text{ \AA}$, $\alpha = 109.038(2)^\circ$, $\beta = 94.423(6)^\circ$, $\gamma = 108.259(9)^\circ$, and $V = 189.03(4) \text{ \AA}^3$. In short, the Li insertion is accompanied by a 7.9% increase in the unit cell volume from 173.7 to 189.0 \AA^3 in accordance with the larger size of Fe^{2+} compared with Fe^{3+} . The expansion is a little larger than that observed for olivine LiFePO_4 on oxidation to FePO_4 (6.7%) and much more than that reported for the transition in the layered $\text{NaFePO}_4\text{F} \leftrightarrow$ layered $\text{Na}_2\text{FePO}_4\text{F}$ of 3.8%.¹⁴ In the latter case, the unique structural features of the very different two-dimensional lattice (Pbcn), which maintains an interlayer Na^+ ion as a “pillar” during redox, enables a quasi-solid solution behavior over the compositional range.

LiFePO_4F exhibits an electrochemical transformation to $\text{Li}_2\text{FePO}_4\text{F}$ (Fig. 4) at an overall potential of roughly 3 V, with a reversible capacity of 0.96 Li corresponding to a specific gravimetric capacity of 145 mAh/g. This is very close to the theoretical capacity of 152 mAh/g for LiFePO_4F . The fact that this can be easily attained without a strict control of particle size or attention to conductive coatings is a clear indication of facile transport in the tavorite framework and the predominant importance of ion conductivity. Furthermore, the material showed an excellent stable cycle performance at both room temperature and 55°C , indicating that it has a very good high temperature cycling stability. The overall potential is lower than the well-known olivine LiFePO_4 (3.4 V), and the discharge–charge profile is quite different. The region from $\text{Li}_{1+x}\text{FePO}_4\text{F}$ ($x = 0\text{--}0.4$) shows a sloping curve centered around 3.1 V, suggestive of a single-phase behavior, followed by a distinct and an abrupt two-phase plateau at 2.8 V for $x > 0.4$ that is characterized by a very low polarization. The voltage is higher than what is recorded for the $\text{Fe}^{3+/2+}$ couple in LiFePO_4OH of ~ 2.5 V.¹⁵ The low polarization and high reversibility indicate a facile phase transformation. Indeed, we found that the chemical oxidation of $\text{Li}_2\text{FePO}_4\text{F}$ (prepared by reduction as described above) fully regenerates LiFePO_4F , as shown by the sequence of XRD patterns in Fig. 5. This can be repeated sequentially with little loss in crystallinity. Thus, although the tavorite phase LiFePO_4F possesses a lower redox voltage than the olivine LiFePO_4 does, which makes it less attractive for some practical applications, it displays intriguing ion conductive pathways and a highly reversible redox reaction on lithium insertion

with a retention of an isostructuralavorite framework. These observations lead to the obvious questions of the nature of the multiple-phase transformations inavorite, the sites occupied on the Li insertion, and the kinetics of Li ion mobility in this interesting 3D ion-pathway lattice. The details of these issues are now under investigation and will be reported subsequently.

Acknowledgments

We are grateful to Professor Dominic Ryan (McGill University, Physics) for the acquisition and fitting of the Mössbauer spectra. We acknowledge the funding from NSERC (Canada) through the Discovery grant and Canada Research Chair programs.

University of Waterloo assisted in meeting the publication costs of this article.

References

1. W. H. Baur, *Heidelb. Beitr. Mineral. Petrogr.*, **6**, 399 (1959).
2. V. I. Simonov and N. V. Belov, *Kristallografiya*, **3**, 429 (1958).
3. A. C. Roberts, P. J. Dunn, J. D. Grice, D. E. Newbury, E. Dale, and W. L. Roberts, *Powder Diffr.*, **3**, 93 (1988).
4. A. Richards, O. Fejerskov, and V. Baelum, *Adv. Dent. Res.*, **3**, 147 (1989).
5. L. Sebastian, J. Gopalkrishnan, and Y. Piffard, *J. Mater. Chem.*, **12**, 374 (2002).
6. J. Barker, M. Y. Saidi, and J. Swoyer, U.S. Pat. 6,387,567 (2002); M. Anji Reddy, V. Pralong, V. Caignaert, U. V. Varadaraju, and B. Raveau, *Electrochem. Commun.*, **11**, 1807 (2009).
7. J. Barker, M. Y. Saidi, and J. Swoyer, *J. Electrochem. Soc.*, **151**, A1670 (2004).
8. J. Barker, M. Y. Saidi, and J. Swoyer, U.S. Pat. 163,669 (2005).
9. S.-C. Yin, P. Subramanya Herle, A. Higgins, N. J. Taylor, Y. Makimura, and L. F. Nazar, *Chem. Mater.*, **18**, 1745 (2006).
10. S. P. Badi, T. N. Ramesh, B. Ellis, K. T. Lee, and L. F. Nazar, Abstract 397, The Electrochemical Society Meeting Abstracts, Vol. 2009-02, Vienna, Austria, Oct 4-9, 2009.
11. A. C. Larson and R. B. V. Dreele, GSAS, Technical Report NM87545, Los Alamos National Laboratory, Los Alamos, New Mexico (1994).
12. D. A. Rusakov, A. A. Filaretov, M. N. Bubentsova, V. P. Danilov, and L. N. Komissarova, *Zh. Neorg. Khim.*, **51**, 922 (2006).
13. N. Recham, J.-N. Chotard, J.-C. Jumas, L. Laffont, M. Armand, and J.-M. Tarascon, *Chem. Mater.*, In press.
14. B. Ellis, W. R. M. Makahnouk, Y. Makimura, K. Toghill, and L. F. Nazar, *Nature Mater.*, **6**, 749 (2007).
15. L. Croguenec, N. Marx, D. Carlier, A. Wattiaux, L. Bourgeois, P. Kubiak, F. LeCras, and C. Delmas, in *Proceedings of the ACS Meeting*, CRM-100, American Chemical Society (2009).